Environ Biol Fish (2009) 85:33–38
DOI 10.1007/s10641-009-9453-z

Retinal topography of ganglion cells in immature ocean sunfish, *Mola mola*

Masakatsu Kino · Taeko Miayzaki · Tetsuo Iwami · Jun Kohbara

Received: 14 June 2008 / Accepted: 27 January 2009 / Published online: 12 February 2009

Abstract The ocean sunfish, *Mola mola*, is the largest known bony fish. Based on prior studies of diet composition, it is considered to be a pelagic zooplanktivore. However, a recent study using acoustic telemetry revealed that they repeatedly dive to depths of >50 m during the day. We examined the distribution of cells within the retinal ganglion cell layer in the immature ocean sunfish (c.a. 50 cm total length) and estimated their visual acuity with respect to the main visual axis and visual fields. Visual acuity was between 3.37 and 4.41 cycles/degree. The region of highest cell density was located in the dorso-temporal retina, indicating that the main visual axis of ocean sunfish is directed towards the lower frontal portion of the visual field. This axis is considered beneficial for detecting prey items when the sunfish are migrating vertically through the water column, and in foraging behavior near the sea bottom.

Keywords *Mola mola* · Ocean sunfish · Retinal ganglion cell · Visual acuity · Main visual axis · Visual field · Retina

M. Kino · T. Miayzaki (✉) · J. Kohbara
Department of Life Sciences,
Graduate School of Bioresources, Mie University,
Tsu, Mie 514-8507, Japan
e-mail: taeko@bio.mie-u.ac.jp

T. Iwami
Tokyo Kasei-Gakuin University,
Machida, Tokyo 194-0292, Japan

Introduction

The ocean sunfish, *Mola mola*, is the largest known bony fish (Gudger 1928; Matsuura and Tyler 1998). They feed primarily on gelatinous zooplankton, so are generally considered to be pelagic zooplanktivores (Fraser-Bruner 1951). However, a recent study using acoustic telemetry found that ocean sunfish (73–151 cm in total length) often dive repeatedly to depths in excess of 50 m during the day. Surprisingly, some individuals were even recorded approaching depths of 400 m (Cartamil and Lowe 2004). In addition, brittle-star and/or flounder have been found in the gut of ocean sunfish. The results of these studies suggest that ocean sunfish sometimes feed on the sea bottom (Bass et al. 2005), challenging the traditional notion that this species is strictly a pelagic zooplanktivore.

The topography of retinal ganglion cells has been investigated in a number of fish species. It has been suggested that the location of peak cell density often reflects both the habitat and main visual axis of feeding behavior (Collin and Pettigrew 1988a, b; Shand et al. 2000). However, the retina of adult or juvenile ocean sunfish has not been examined to date. The large body size of ocean sunfish, especially adults, makes sampling and/or holding of specimens problematic for histological studies. We studied the retinal histology of immature ocean sunfish by measuring the density of cells within the retinal ganglion cell layer and estimating

Table 1 Summary of counts of cells within the retinal ganglion cell layer and calculation of visual acuity in four retinas of ocean sunfish

		Eye diameter (m)	Retinal surface area (mm^2)	Counted points	Av. cell density ($cells/mm^2$)	Total cell no.	D ($cell/mm^2$)	Lens diameter (m)	PND (m)	SRP (cycles/degree)
Mola-1	Left	35.2	1,072	318	11.8×10^2	126×10^4	2,160	8.38	10.68	4.33
Mola-2	left	33.3	724	192	10.6×10^2	765×10^3	2,192	8.46	10.79	4.41
Mola-3	Left	35.4	916	290	7.9×10^2	724×10^3	1,296	8.41	10.72	3.37
	right	33.8	1,028	303	8.1×10^2	833×10^3	1,408	8.41	10.72	3.51

their main visual axis and anatomical spatial resolving power (SRP). Based on the retinal topography we make inferences regarding the behavior and biology of this species.

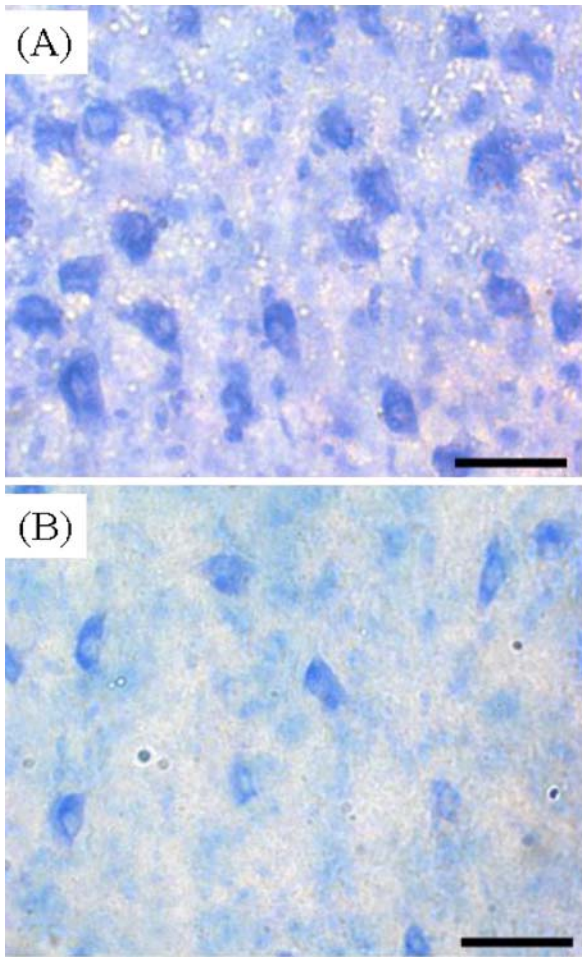

Fig. 1 Photographs of ganglion cells from the right retina of Mola-3. **A** The high density region in the dorso-temporal margin and **B** the low density region in the nasal retina. Scale bar: 30 μm

Materials and methods

Three *Mola mola* specimens were obtained from fishermen at the Shimakatsu fishing port, Mie-Prefecture, Japan on 19 December 2005 (Mola-1: 423 mm total length, 3.3 kg body weight; Mola-2: 430 mm total length, 3.4 kg body weight) and on 27 March, 2006 (Mola-3: 455 mm total length, 3.5 kg body weight). These specimens were relatively young, immature fish (Nakatsubo et al. 2007). We took photographs of the dorsal, lateral, and frontal aspects of the specimens to determine their body profile and eye position relative to the body.

A solution of 10% formalin was injected into the bulbus arteriosus to achieve perfusion fixation. The specimens were then post-fixed by immersion in 20% formalin for a week. The left eyeballs of Mola-1 and Mola-2 and both the left and right eyeballs of Mola-3 were used and the retinas were flat mounted by making peripheral incisions. Whole-mount preparations of each retina were then made following the protocol of Ito and Murakami (1984). The unstained flat mounted retinas were scanned. Shrinkage may occur during retinal whole-mount preparation, presumably due to fixation and dehydration. We estimated the shrinkage caused by staining by comparing post-stain images with the original scans. We were not able to evaluate the occurrence of shrinkage due to fixation.

Each retina was then divided into five segments, centered at the optic papilla. Each of the retinal segments were glued onto a gelatinized slide with the ganglion cell layer facing upwards, and stained with cresyl-violet, dehydrated, and mounted in EUKITT (O. Kindler GmbH and Co., Germany). The number of ganglion cells per 0.25×0.25 mm area was counted at 2 mm intervals across all the retinal pieces, under a light microscope using an ocular micrometer. We

sampled 318, 192, 290, and 303 points on the left retinas of Mola-1 and Mola-2 and the left and right retinas of Mola-3, respectively (Table 1). The position of each point was mapped onto the scan of the original retina. The counts of cells within the retinal ganglion cell layer were converted to give the number of cells/mm^2. Finally, isodensity contour maps of the cells within the retinal ganglion cell layer were constructed for each of the four retinas. Anatomical SRP was calculated from the maximum ganglion cell density (D). The posterior nodal distance (PND) of the eye was derived by multiplying the lens radius (r: mm) and Matthiessen's ratio (2.55), i.e. PND=2.55r (Collin and Pettigrew 1989).

Results and discussion

The diameter of the four eye balls ranged from 33.3 mm to 35.4 mm and retinal surface area was between 724 mm^2 and 1,072 mm^2 (Table 1). Ganglion cells were non-uniformly distributed across the retina (Fig. 1). The average cell density estimated from the counts of cells within the retinal ganglion cell layer was between 7.9×10^2 and 11.8×10^2 cells mm^{-2}.

The topographical distribution of ganglion cells differed among the four retinas. However, the region of highest density was always located at the dorso-temporal margin (Fig. 2). Nissl-staining with cresyl-violet stains both ganglion cells and a population of non-ganglion cells ('displaced' amacrine cells). Therefore, the calculations of cell density may be overestimated. However we expect that the topographic patterns we observed would be unchanged if non-ganglion cells are in included the cell counts (Bailes et al. 2006). The peak density of cells in the left retinas of Mola-1 and Mola-2 was 2,160 and 2,192 cells mm^{-2}, respectively. The peak density of cells in the left and right retinas of Mola-3 was 1,296 and 1,408 cells mm^{-2}, respectively (Table 1). The lowest density of ganglion cells was measured near the nasal region of the retina (Fig. 2); where cell density was between 272 and 544 cells mm^{-2}.

In general, the visual axis of a fish is defined as the direction linking the center of the lens and the retinal

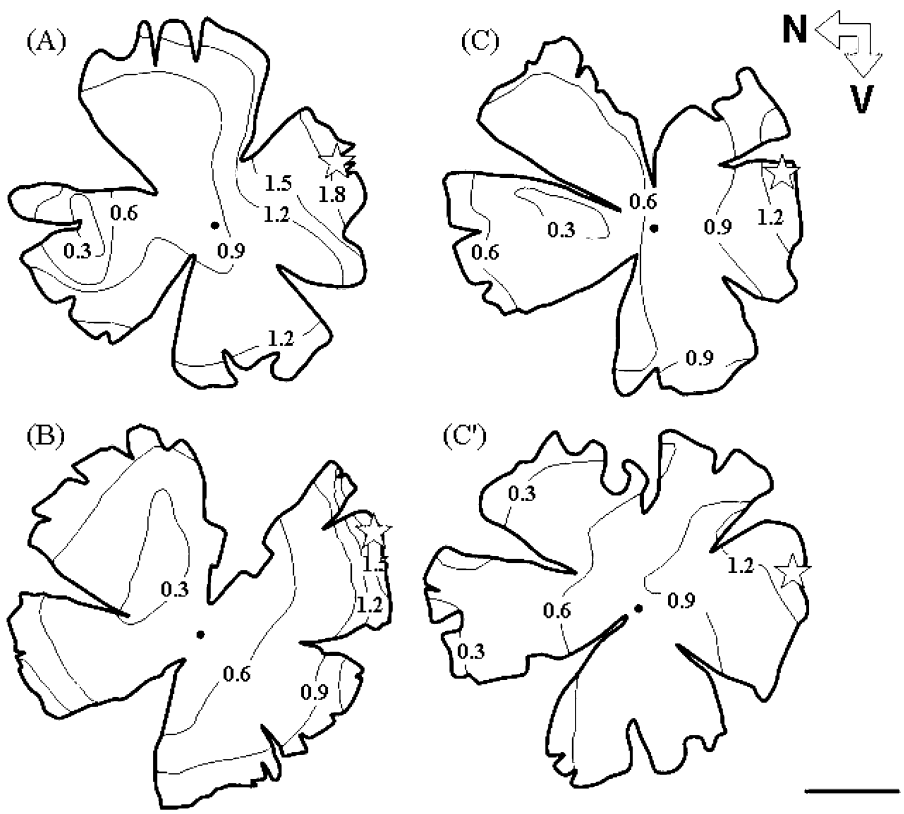

Fig. 2 Isodensity contour maps showing the distribution of Nissl-stained neurons (retinal ganglion and displaced amacrine cells) located within the ganglion cell layer in the left retina of Mola-1 (**A**), the left retina of Mola-2 (**B**), and the left (**C**) and right (**C'**) retinas of Mola-3. All cell densities × 10^3 mm^2. *N* = nasal; *V* = ventral. The symbols (•) indicate the position of the optic papilla and the stars depict the position of the localized peak in cell density. Scale bar: 1 cm

positions with the highest cell density (Tamura 1957). Deciding certain position of lens center in the retinal whole-mount image is difficult. We used a direction to the opposite side of the retina from the position of the region of peak cell densities passing through the optic nerve head. Thus, we estimated that the main visual axis was directed towards the lower frontal portion of the visual field (10–20 degrees below the horizon) (Fig. 3A). Furthermore, the estimated field of best vision, defined as the area containing ganglion cell density at 75% of maximum values (Heffner and Heffner 1992) was at approximately 80 degrees (Fig. 3A).

The monocular field of best vision was estimated using the area of highest cell density and the pupillary plane of the eye, which was measured from the dorsal fish profile (Fig. 3B). The highest density angle in the eye cup cross section was calculated as the average ratio of the width of the area with >75% cell density to the total retina width for all four retinas (Fig. 3A). This value occurs within an angle of about 36 degrees in the forward direction relative to the body axis of the fish (Fig. 3B). The binocular visual field, based on the relationship between body morphology and eye position, was estimated to be ~30 degrees, and the

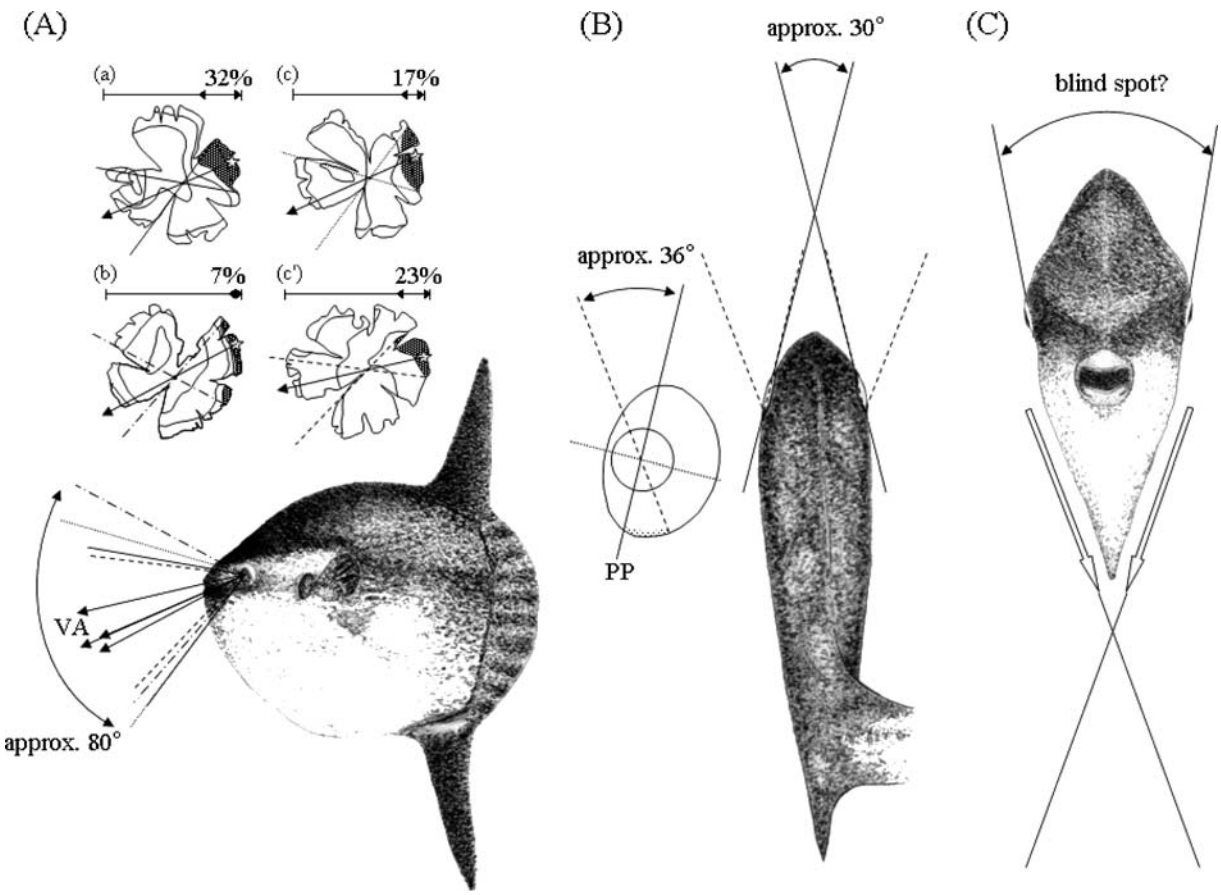

Fig. 3 Schematic diagram of the visual field of the ocean sunfish. The images were traced from photographs of Mola-3. **A** Lateral view of the binocular visual field based on the distribution of cells within the retinal ganglion cell layer. Topographical contour maps of **a**, **b**, **c**, and **c**' are copies of Fig. 2-**A**, **B**, **C** and **C**', respectively. The meshed area indicates the area where ganglion cell density is >75% of maximum. Presumptive visual axis (VA) was estimated from the position of the region of peak cell densities passing through the optic nerve head in place of the center of the lens. **B** Dorsal view of the binocular visual field, based on the eye position, and the monocular visual field, based on the area of >75% cell density (indicated by the *dashed line* in the enlarged schematic left eyeball). PP = pupillary plane of the eye. **C** Frontal view of the head showing the blind spot above the head which was estimated based on eye position and body shape. *White arrows* indicate the direction of light penetration under which ocean sunfish are camouflaged

monocular visual field was as wide as 180 degrees within the lateral plane (Fig. 3B).

Cartamil and Lowe (2004) showed that ocean sunfish often dive to depths of 40–150 m for short durations (about 10 min) during the daytime. They hypothesized that this diurnal diving behavior is a means of foraging for prey items that migrate vertically. Taken together with the results of our study and the location of the main visual axis, we suggest that ocean sunfish detect their prey items during their descent through the water column. In addition, the visual axis might also be effective for foraging near the sea bottom.

Ocean sunfish are able to cover a large distance during a single day (26.8 km day^{-1}) and their movements are often highly directional (Cartamil and Lowe 2004). The position of peak cell density is typically related to the habitat and/or main visual axis for feeding. We hypothesize that the direction of the visual axis and visual field may also aid in migratory movements in ocean sunfish. Eye movements, particularly in the ventral plane, were observed in the live specimens (Fig. 4). Such movement may change both the visual field and the main visual axis.

When observed from the front, the ocean sunfish is rhomboidal in cross section. The eyes are positioned such that the visual field is blocked dorsally (Fig. 3C). Thus, the ocean sunfish may have a blind spot dorsally due to the protuberance of the upper margin of the eyes. Given this, the ocean sunfish is potentially vulnerable to an attack from above. It is thought that the sunfish address this issue behaviorally by swimming with a horizontal incline (Matsuura and Tyler 1998) which would allow them to alter their visual field. The dark back and lighter belly (counter shading) are also adaptations that reduce their visibility to predators/prey in the open ocean. The ventral region is shaped like an inverted triangle with an acute angle at the tip, which may also reduce the ability of predators to detect the ocean sunfish from below (Fig. 3C).

The parameters calculated from peak cell densities are shown in Table 1. The SRPs were 4.33, 4.41, 3.37, and 3.51 cycles per degree for the Mola-1 left retina, Mola-2 left retina, and Mola-3 left and right retinas, respectively. Retinal shrinkage following staining was between 8% to 10%. However, the decrease in the estimated maximum SRP due to shrinkage was less than 0.21 cycles per degree.

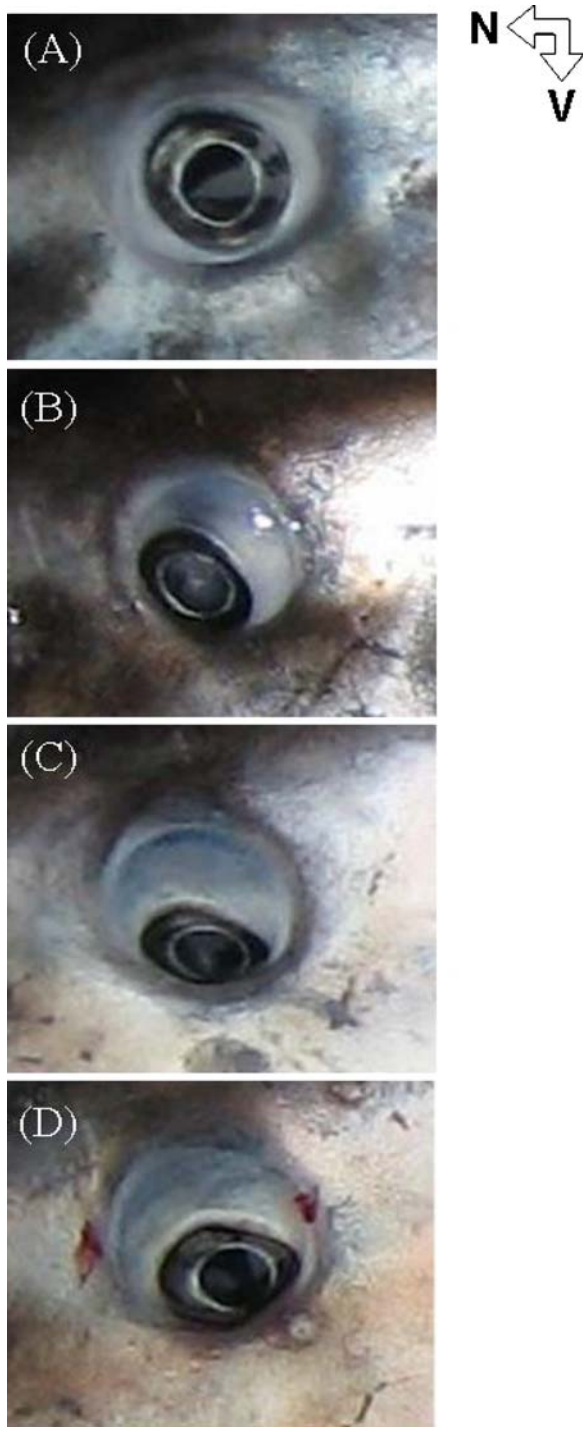

Fig. 4 Photographs of eye movement in ocean sunfish (Mola-3). **A** directed laterally, **B** directed anterio-ventrally, **C** directed ventrally, and **D** directed tempro-ventrally. *N* = nasal; *V* = ventral

The SRP of immature ocean sunfish is comparable to that measured (calculated using the peak ganglion cell densities) in several adult sharks (3.7, *Scyliorhinus canicula*; 3.8, *Galeus melastomus*; and 2.8 cycles per degree, *Etmopterus spinax*: Bozzano and Collin 2000), and slightly higher than adult cetaceans (3.3, *Pseudorca crassidens*; 2.7, *Lagenorhynchus obliquidens*; 2.6 cycles per degree, *Delphinapterus leucas*: Murayama and Somiya 1998), but much lower than the adult marlin (8.5 cycles per degree, *Makaira nigricans*: Fritsches et al. 2003). However, it is well known that the visual acuity of fish increases with growth in size (Hariston et al. 1982; Miyazaki et al. 2000; Shand et al. 2000). The largest ocean sunfish specimen recorded to date measured in excess of 3 m (Nelson 2006). Therefore, the visual acuity we report may change as the animal grows.

We know very little regarding the ecology of ocean sunfish due to the difficulties associated with observing their behavior in their natural environment. To better understand their life history, retinal histology at the larval, juvenile, and adult stages may provide insights into behavior that can be combined with the results of biotelemetry studies.

Acknowledgements This study was supported by the Tokai Art and Science Foundation (2005) and a Grant-in-Aid for Scientific Research from the JSPS (No. 17570077). We thank Noriaki Yamashita and staff of the Shimakatsu Oshiki Co. Ltd. for allowing us to obtain the ocean sunfish.

References

Bailes HJ, Trezise AEO, Collin SP (2006) The number, morphology, and distribution of retinal ganglion cells and optic axons in the Australian lungfish *Neoceratodus forsteri* (Krefft 1870). Vis Neurosci 23:257–273. doi:10.1017/S0952523806232103

Bass AL, Dewar H, Thys T, Streelman JT, Karl SA (2005) Evolutionary divergence among lineages of the ocean sunfish family, Molidae (Tetradontiformes). Mar Biol (Berl) 148:405–414. doi:10.1007/s00227-005-0089-z

Bozzano A, Collin SP (2000) Retinal ganglion cell topography in elasmobranchs. Brain Behav Evol 55:191–208. doi:10.1159/000006652

Cartamil DP, Lowe CG (2004) Diel movement patterns of ocean sunfish *Mola mola* off southern California. Mar Ecol Prog Ser 266:245–253. doi:10.3354/meps266245

Collin SP, Pettigrew JD (1988a) Retinal topography in reef teleosts. I. Some species with well-developed areae but poorly-developed streaks. Brain Behav Evol 31:269–282. doi:10.1159/000116594

Collin SP, Pettigrew JD (1988b) Retinal topography in reef teleosts. II. Some species with prominent horizontal streaks and high-density areae. Brain Behav Evol 31:283–295. doi:10.1159/000116595

Collin SP, Pettigrew JD (1989) Quantitative comparison of the limits on visual spatial resolution set by the ganglion cell layer in twelve species of reef teleosts.. Brain Behav Evol 34:184–192. doi:10.1159/000116504

Fraser-Bruner A (1951) The ocean sunfishes (Family Molidae). Bull Br Mus Nat Hist 1:89–121

Fritsches KA, Marshall NJ, Warrant EJ (2003) Retinal specializations in the blue marlin: eyes designed for sensitivity to low light levels. Mar Freshw Res 54:333–341. doi:10.1071/MF02126

Gudger EW (1928) Capture of an ocean sunfish. Sci Mon 26:257–261

Hariston NG Jr, Li KT, Easter SS Jr (1982) Fish vision and the detection of planktonic prey. Science 218:1240–1242. doi:10.1126/science.7146908

Heffner RS, Heffner HE (1992) Visual factors in sound localization in mammals. J Comp Neurol 317:219–232. doi:10.1002/cne.903170302

Ito H, Murakami T (1984) Retinal ganglion cells in two teleosts species, *Sebastiscus marmoratus* and *Navodon modestus*. J Comp Neurol 229:80–96. doi:10.1002/cne.902290107

Matsuura K, Tyler JC (1998) Triggerfishes and their allies. In: Paxton JR, Eschmeyer WN (eds) Encyclopedia of fishes. Academic Press, San Diego, pp 227–231

Miyazaki T, Shiozawa S, Kogane T, Masuda R, Maruyama K, Tsukamoto K (2000) Developmental changes of the light intensity threshold for schooling formation in the striped jack *Pseudocaranx dentex*. Mar Ecol Prog Ser 192:267–275. doi:10.3354/meps192267

Murayama T, Somiya H (1998) Distribution of ganglion cells and object localizing ability in the retina of three cetaceans. Fish Sci 64:27–30

Nakatsubo T, Kawachi M, Mano N, Hirose H (2007) Estimation of maturation in wild and captive ocean sunfish *Mola mola*. Aquac Sci 55:259–264

Nelson JS (2006) Fishes of the world, 4th edn. John & Sons Inc, Hoboken, New Jersey

Shand J, Chin SM, Harman AM, Moore S, Collin SP (2000) Variability in the location of the retinal ganglion cell area centralis is correlated with ontogenetic changes in feeding behavior in the black bream, *Acanthopagrus butcheri* (Sparidae, Teleostei). Brain Behav Evol 55:176–190. doi:10.1159/000006651

Tamura T (1957) A study of visual perception in fish, especially on resolving power and accommodation. Bull Jap Soc Sci Fish 22:536–557